Proceedings of the International Heat Transfer Conference
IHTC14
August 8-13, 2010, Washington, DC, USA

IHTC14-23050

EFFECT OF ENERGY DEPOSITION MODES ON ULTRAFAST SOLID-LIQUID-VAPOR PHASE CHANGE OF A THIN GOLD FILM IRRADIATED BY A FEMTOSECOND LASER

Jing Huang, Yuwen Zhang[1,2,3], and J.K. Chen[2,3]
Department of Mechanical and Aerospace Engineering
University of Missouri
Columbia MO 65211, USA

Mo Yang[3]
College of Energy and Power Engineering
University of Shanghai for Science and Technology
Shanghai 200093, China

ABSTRACT

Effects of different parameters on the melting, vaporization and resolidification processes of thin gold film irradiated by a femtosecond pulse laser are systematically studied. The classical two-temperature model was adopted to depict the non-equilibrium heat transfer in electrons and lattice. The melting and resolidification processes, which was characterized by the solid-liquid interfacial velocity, as well as elevated melting temperature and depressed solidification temperature, was obtained by considering the interfacial energy balance and nucleation dynamics. Vaporization process which leads to ablation was described by tracking the location of liquid-vapor interface with an iterative procedure based on energy balance and gas kinetics law. The parameters in discussion include film thickness, laser fluence, pulse duration, pulse number, repetition rate, pulse train number, etc. Their effects on the maximum lattice temperature, melting depth and ablation depth are discussed based on the simulation results.

INTRODUCTION

Ultrashort pulsed laser is regarded to be an ideal tool for high-resolution, high-quality material processing, fast fabrication and diagnostic because of its ability to deposit high density energy at a given place in a very short period of time. The heat flux of a nanosecond laser pulse can reach as high as 10^{12} w/m^2, while a femtosecond one can reach 10^{21} w/m^2. Such a rapid and highly energy densified process leads to unique characteristics to be studied. The traditional phenomenological laws, such as Fourier's law, assume that heat transfer takes place simultaneously with the onset of temperature gradient. During pico- to femtosecond laser-materials processing, the characteristic times of the heat carriers are comparable to the characteristic energy excitation time [1]. The Fourier's law becomes invalid for such ultrafast process. In the last two decades, many researchers worked on this problem, to uncover the heat transfer mechanism with extremely short time-scale and high energy intensity [2-6]. Various computational models were put forward and developed to describe the non-equilibrium energy transport phenomena during the process. One of the classical methods is the two-temperature model, which was originally proposed by Anisimov [7] and then rigorously derived by Qiu and Tien [8] based on the Boltzmann equation. The nonequilibrium energy transport between electron and lattice can also be described by the dual-phase-lag model [9, 10]. Jiang and Tsai extended the existing two-temperature model to high electron temperatures by using full-run quantum treatments [11]. Chen et al. proposed a semiclassical two-step heating model to investigate thermal transport in metals caused by ultrashort laser irradiation [12].

Most existing two-temperature models dealt with the case that lattice temperature is well below the melting point and only pure conduction is considered. Under higher laser fluence and/or short pulse, the lattice temperature can exceed the melting point and melting takes place. The liquid phase will be resolidified when the lattice is cooled by conducting heat away. The rapid phase change phenomena induced by ultrashort pulse laser are controlled by nucleation dynamics at the interface, not by interfacial energy balance [13]. Zhang and Chen [14] proposed an implicit, fixed grid interfacial tracking method to solve kinetics controlled rapid melting and resolidification

[1] Corresponding author. zhangyu@missouri.edu
[2] Fellow ASME
[3] Professor

during ultrashort pulse laser interaction with a free-standing metal film. The nonlinear electron heat capacity obtained by Jiang and Tsai [11] and a temperature-dependent electron-lattice coupling factor based on a phenomenological model [15] is incorporated into the interfacial tracking method. When the laser fluence is sufficiently high or when the laser pulse width is in the order of femtosecond, the liquid surface temperature may exceed the saturation temperature and vaporization may take place. Chowdhury and Xu [16] proposed a numerical model to simulate the melting-vaporization-resolidification process during femtosecond laser-metal interaction, which will be adopted in our work to track the liquid-vapor interface.

In this work, the entire process of laser-metal interaction – including preheating, melting, vaporization, resolidification and thermalization – will be thoroughly investigated under the frame works of two-temperature model and interfacial tracking method. Temperature and velocity of liquid-vapor interface are controlled by energy balance and gas kinetics law, which will be fulfilled simultaneously through an iterative computational procedure. At the mean time, the effects of various parameters on the maximum lattice temperature, melting depth and ablation depth are discussed based on the simulation results. The parameters in discussion include film thickness, laser fluence, pulse duration, pulse number, repetition rate, pulse train number, etc.

NOMENCLATURE

Be	coefficient for electron heat capacity (J/m^3-K^2)
C	heat capacity (J/m^3-K)
c_p	specific heat (J/kg-K)
f_{rep}	repetition rate (Hz)
G	electron-lattice coupling factor (W/m^3-K)
h	latent heat of phase change (J/kg)
J_i	single pulse fluence (J/cm^2)
J_t	total energy of a pulse train (J/cm^2)
k	thermal conductivity (W/m-K)
L	thickness of the metal film (m)
M	molar mass (kg/kmol)
q''	heat flux (W/m^2)
R	reflectivity
R_g	specific gas constant (J/kg-K)
R_u	universal gas constant (J/kmol-K)
s	interfacial location (m)
S	intensity of the internal heat source (W/m^3)
t	time (s)
t_p	pulse width (s)
t_{sep}	separation time (s)
T	temperature (K)
T_F	Fermi temperature (K)
T_m	melting point (K)
u	interfacial velocity (m/s)
V_0	interfacial velocity factor (m/s)
x	coordinate (m)

Greek Symbols

δ	optical penetration depth (m)
δ_b	ballistic range (m)
ε	total emissivity
ρ	density (kg/m^3)
σ	Stefan–Boltzmann constant (W/m^2-K^4)

Superscripts

0	last time step

Subscripts

0	initial condition
e	electron
eq	thermal equilibrium state
i	pulse sequence
l	lattice
ℓ	liquid
R	thermal radiation
s	solid
$s\ell$	solid-liquid interface
sur	surface
∞	ambient environment

PHYSICAL MODEL

Figure 1 shows the physical model of the problem under consideration. Laser pulses impinge on the right side of a free standing gold film, which has a thickness of L. The range of thickness used in this paper is very small in comparison to the radius of the laser beam; therefore the problem under discussion can be approximated to be one-dimensional. The structures of three modes of laser pulses used in this paper is shown in Fig. 2, in which f_{rep} and t_{sep} are the repetition rate and time interval between single pulses, respectively. Each single pulse is assumed to be temporally Gaussian. The pulse duration (t_p), defined as the full width at half maximum (FWHM).

The two-step heating model for free electrons and the lattice are given by [7]

$$C_e \frac{\partial T_e}{\partial t} = \frac{\partial}{\partial x}\left(k_e \frac{\partial T_e}{dx} \right) - G(T_e - T_l) + S \tag{1}$$

$$C_l \frac{\partial T_l}{\partial t} = \frac{\partial}{\partial x}\left(k_l \frac{\partial T_l}{dx} \right) + G(T_e - T_l) \tag{2}$$

The heat capacity of electron C_e is approximated by [12]

$$C_e = \begin{cases} B_e T_e, & T_e < T_F/\pi^2 \\ 2B_e T_e/3 + C_e'/3, & T_F/\pi^2 \le T_e < 3T_F/\pi^2 \\ Nk_B + C_e'/3, & 3T_F/\pi^2 \le T_e < T_F \\ 3Nk_B/2, & T_e \ge T_F \end{cases} \tag{3}$$

where

$$C_e' = B_e T_F/\pi^2 + \frac{3Nk_B/2 - B_e T_F/\pi^2}{T_F - T_F/\pi^2}\left(T_e - T_F/\pi^2 \right) \tag{4}$$

The thermal conductivity of electron k_e can be obtained from [17]

$$k_e = \chi \frac{\left(\vartheta_e^2 + 0.16 \right)^{5/4} \left(\vartheta_e^2 + 0.44 \right) \vartheta_e}{\left(\vartheta_e^2 + 0.092 \right)^{1/2} \left(\vartheta_e^2 + \eta \vartheta_l \right)} \tag{5}$$

where $\vartheta_e = T_e/T_F$ and $\vartheta_l = T_l/T_F$.

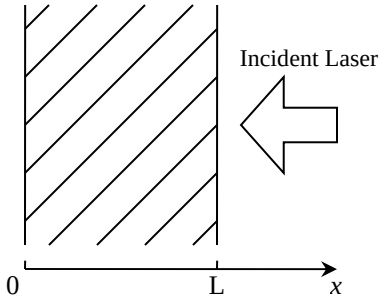

Fig. 1 Laser irradiation on thin film

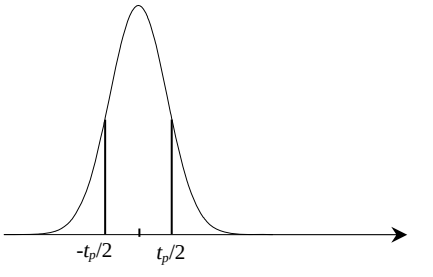

(a) Single laser pulse

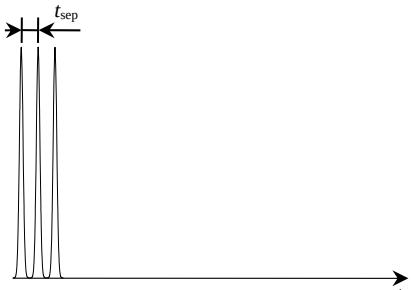

(b) Multiple Pulses

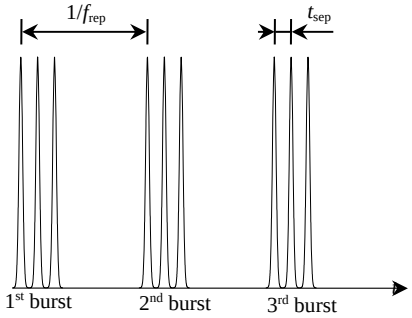

(c) Laser Pulse Train

Fig. 2 Three different laser modes

In eqs. (1) and (2), G is the electron-lattice coupling factor. A phenomenological temperature-dependent G suggested by Chen et al. [15] is adopted:

$$G = G_{RT}\left[\frac{A_e}{B_1}\left(T_e + T_l\right) + 1\right] \tag{6}$$

where GRT is the coupling factor at room temperature; A_e and B_l are material constants for the electron relaxation time.

Since the electrons are more likely to collide with liquid atoms than the atoms in solid crystals, in the liquid phase, G is taken to be 20% higher than that of the solid [18].

The laser irradiation is considered as a source term S in eq. (1):

$$S = \sum_{i=1}^{K}\sum_{j=1}^{N} \frac{0.94 J_i \left(1-R\right)}{t_p\left(\delta+\delta_b\right)\left[1-e^{-L/(\delta+\delta_b)}\right]} \cdot \exp\left[-\frac{x}{\left(\delta+\delta_b\right)} - 2.77\left(\frac{t-\frac{i-1}{f_{rep}}-(j-1)t_{sep}}{t_p}\right)^2\right] \tag{7}$$

where K is the number of pulse trains, N is the number of pulses in each train, t_{sep} is separation time between each single pulse, f_{rep} is the repetition rate, R is the reflectivity of the thin film, δ is the optical penetration depth, J is the laser pulse fluence, δ_b is the for the ballistic depth, and $[1-e^{-L/(\delta+\delta_b)}]$ is to correct the finite film thickness effect. For single pulse irradiation, K and N are all set to be 1. For multiple pulse irradiations, K is set to be 1.

For a metal at its thermal equilibrium state, the thermal conductivity, k_{eq}, is the sum of the electron thermal conductivity, k_e, and the lattice thermal conductivity, k_l. In most cases k_e dominates k_{eq} because free electrons contribute to the majority part of heat conduction, For gold, k_l is usually taken to be 1% of k_{eq} [19], i.e.,

$$k_l = 0.01 k_{eq} \tag{8}$$

A uniform temperature distribution is set to be the initial condition:

$$T_e\left(x,-2t_p\right) = T_l\left(x,-2t_p\right) = T_0 \tag{9}$$

On the right side of the film which receives laser energy, the heat loss caused by radiation will be considered while on the other side adiabatic boundary condition is applied:

$$\left.\frac{\partial T_e}{\partial x}\right|_{x=0} = \left.\frac{\partial T_e}{\partial x}\right|_{x=L} = \left.\frac{\partial T_l}{\partial x}\right|_{x=0} = 0 \tag{10}$$

$$\left.q_R''\right|_{x=L} = \sigma\varepsilon(T_{sur}^4 - T_\infty^4) \tag{11}$$

Before evaporation takes place, T_{sur} is the surface lattice temperature at $x = L$. After evaporation begins, T_{sur} is the liquid-vapor interface temperature, which varies with the heating condition.

The energy balance at the solid-liquid interface is [20]:

$$k_{l,s}\frac{\partial T_{l,s}}{\partial x} - k_{l,\ell}\frac{\partial T_{l,\ell}}{\partial x} = \rho_\ell h_m u_{s\ell} \qquad x = s(t) \tag{12}$$

where $T_{l,s}$ and $T_{l,\ell}$ are solid and liquid lattice temperature respectively, ρ is mass density, h_m is latent heat of fusion, and u_s is solid-liquid interfacial velocity. The additional interfacial velocity due to the density change during melting and resolidification has been considered.

For rapid melting and solidification processes, the velocity of the interface is dominated by nucleation dynamics, instead by the energy balance, eq.(12). For ultrashort-pulsed laser melting of gold, the velocity of the solid-liquid interface is [18]

$$u_{s\ell} = V_0\left[1-\exp\left(-\frac{h_m}{R_g T_m}\frac{T_{l,I}-T_m}{T_{l,I}}\right)\right] \tag{13}$$

where V_0 is the maximum interface velocity, R_g is the gas constant for the metal, and $T_{l,I}$ is the interfacial temperature. The interfacial temperature, $T_{l,I}$, is higher than the normal melting point, T_m, during melting and lower than T_m during solidification.

To characterize the vaporization process, Clausius-Clapeyron equation is employed to describe the slope of saturation pressure-temperature curve, with the assumption of ideal gas and thermal equilibrium:

$$\frac{dp}{dT_{\ell v}} = \frac{p h_{\ell v}(T_{\ell v})}{R_u T_{\ell v}^2} \tag{14}$$

where R_u is the universal gas constant, which is related to boiling temperature $T_{\ell v}$ as:

$$h_{\ell v}\left(T_{\ell v}\right) = h_{\ell v 0}\left[1-\left(\frac{T_{\ell v}}{T_c}\right)^2\right]^{1/2} \tag{15}$$

where $h_{\ell v 0}$ is the latent heat of vaporization at absolute zero and T_c the critical temperature [21]. By integrating eq.(14), the relationship between interfacial temperature and pressure can be obtained as:

$$p = p_0 \exp\left\{\begin{array}{l} -\frac{\rho_\ell L_0}{R_u}\left[\frac{1}{T_{\ell v}}\sqrt{1-\left(\frac{T_{\ell v}}{T_c}\right)^2}-\frac{1}{T_b}\sqrt{1-\left(\frac{T_b}{T_c}\right)^2}\right] \\ -\frac{\rho_\ell L_0}{R_u T_c}\left[\sin^{-1}\left(\frac{T_{\ell v}}{T_c}\right)-\sin^{-1}\left(\frac{T_b}{T_c}\right)\right] \end{array}\right\} \tag{16}$$

The molar evaporation flux j_v at the surface can be calculated by Hertz-Knudsen-Langmuir equation derived from kinetic theory of gases [22],

$$j_v = \frac{Ap}{\sqrt{2\pi M R_u T_{\ell v}}} \tag{17}$$

where A is an accommodation coefficient that shows which portion of vapor molecules striking the liquid-vapor surface is absorbed by this surface [23]. Xu et al. [21] recommended a value of 0.82 for this coefficient. The liquid-vapor interfacial velocity can be obtained from j_v as given below:

$$u_{\ell v} = \frac{M j_v}{\rho_\ell} = \frac{AMp}{\rho_\ell\sqrt{2\pi M R_u T_{\ell v}}} \tag{18}$$

Detailed information and discussion on the evaporation model can be found in our previous work [24, 25]. It should be noted that because multiple pulses and pulse train irradiation will significantly decrease the maximum temperature, within the parameter range being studied in this paper, only single pulse mode will cause evaporation to take place.

NUMERICAL MODEL

The governing equations (1) and (2) are discretized by the Finite Volume Method [26]. A fixed uniform grid with 2050 control volumes is adopted. The time step is variable in the numerical solution. The smallest time step is $10^{-2}t_p$, which is implemented during ($-2t_p$, $2t_p$) of each single pulse. The largest time step is $10^4 t_p$, which is implemented when the difference between electronic and lattice temperature is less than 1K. Thermophysical properties used in the calculations are tabulated in Table 1.

In each time step, an iterative procedure will be employed to deal with the nonlinear relationship between electron energy equation, lattice energy equation, solid-liquid and liquid-vapor interfaces. Electron energy equation (1) is solved first using tri-diagonal matrix method (TDMA), and then the lattice energy equation (2) is solved. After obtaining an estimated electron and lattice temperature field, the velocity and temperature of solid-liquid interface is obtained by using the method provided in Ref. [14] and is briefly described here:

(1) The solid-liquid interfacial temperature T_{sl} is assumed and the solid-liquid phase interfacial velocity is determined according to the interfacial energy balance;

(2) The interfacial velocity from the nucleation dynamics is obtained from Eq.(13);

(3) The interfacial velocities got from Steps (1) and (2) are compared. If the interfacial velocity obtained from the energy balance is higher than that from the nucleation dynamics, the interfacial temperature will be increased; otherwise, the interfacial temperature is decreased.

Steps 1-3 are repeated until the difference between the interfacial velocities obtained from the two methods is less than 10^{-5} m/s.

The following iterative procedure will be employed to track the liquid-vapor interface:

(1) Assume an interfacial velocity $V_{\ell v}^*$, then the new interface location $s_{\ell v}^*$ is determined;

(2) Solve the energy balance equation at the liquid-vapor interface to obtain the interface temperature $T_{\ell v}$;

(3) According to eqs. (16) and (18), obtain the new interface velocity $V_{\ell v}^{**}$;

(4) Go to step 2 and use $V_{\ell v}^{***}$ as the new interface velocity. Steps 2-4 are repeated until the difference between the interfacial velocities obtained from two consecutive iterations is less than 10^{-5}m/s.

RESULTS AND DISCUSSION

1. Vaporization, melting and resolidification of gold film with single pulse irradiation

The melting, evaporation and resolidification processes caused by single pulse irradiation are studied first. For a single pulse of 0.5 J/cm^2, the evolution of surface electron temperature, lattice temperature, solid-liquid interface velocity and location, liquid-vapor interface velocity and location are shown in Fig. 3. It can be seen that electron temperature

increases rapidly due to the depositing of laser energy on electrons. Tens of picoseconds later, the lattice temperature increase to a peak caused by the collision of hot electrons with lattices. During this process, melting and evaporation takes place due to the high lattice temperature. After the temperature peak, heat is conducted into the deeper part of the metal film, and surface temperature decrease gradually. Material ablation caused by evaporation stops and a thin layer of metal is lost due to evaporation. After a maximum melting depth is reached, then melting ceases and material will be resolidified.

Table 1 Thermophysical and optical properties of gold

Coefficient for electronic heat capacity, B_e		70[8]
Material constant, A_e		1.2×10^{7}[15]
Material constant, B_1		1.23×10^{11}[15]
Electron-lattice coupling factor at room temperature, G_{RT} (W/m^3 K)	Solid	2.2×10^{16}[15]
	Liquid	2.6×10^{16}[15]
Specific heat, C_p (J/kg K)	Solid	$105.1+0.2941T_1-8.731\times10^{-4}T_1^2+1.787\times10^{-6}T_1^3-7.051\times10^{-10}T_1^4+1.538\times10^{-13}T_1^5$[15]
	Liquid	163.205[18]
Latent heat of evaporation at T_b, h_{lv} (J/kg)		1.698×10^{6}[27]
Latent heat of fusion, h_m (J/kg)		6.373×10^{4}[27]
Molar weight, M (kg/kmol)		196.967[27]
Reflection coefficient, R		0.6
Universal gas constant, R_u (J/K kmol)		8314.0
Boiling temperature, T_b (K)		3127
Critical temperature, T_c (K)		5590
Melting temperature, T_m (K)		1336
Fermi temperature, T_F (K)		6.42×10^{4}
Limit velocity , V_0 (m/s)		1300[18]
Coefficient for electronic conductivity, χ (W/m K)		353[17]
Optical penetration depth, δ (nm)		20.6
Ballistic range, δ_b (nm)		105[18]
Thermal conductivity at equilibrium, k_{eq} (W/m K)	Solid	$320.973-0.0111T_1-2.747\times10^{-5}T_1^2-4.048\times10^{-9}T_1^3$
	Liquid	$37.72+0.0711T_1-1.721\times10^{-5}T_1^2+1.064\times10^{-9}T_1^3$
Density, ρ (kg/m^3)	Solid	19.3×10^{3}
	Liquid	17.28×10^{3}

With pulse fluence ranged from 0.2 J/cm^2 to 0.7 J/cm^2, the relationship between maximum lattice temperature and maximum melting depth is shown in Fig. 4. Obviously, higher pulse fluence leads to a deeper melting. Figures 4 will serve as the base of the comparison between multiple pulses and single pulse. If the resultant point of a multiple pulses is located in the upper part of Fig. 4, it means with the same maximum temperature, multiple pulses will achieve deeper melting, and vice-versa.

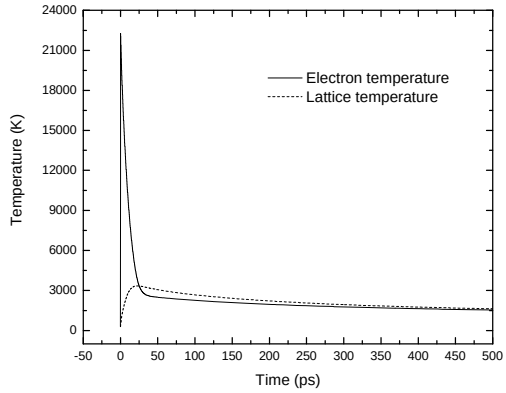

(a) Electron and lattice temperature

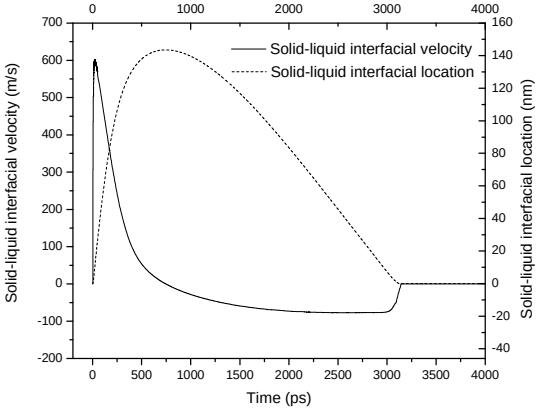

(b) Solid-liquid interfacial velocity and location

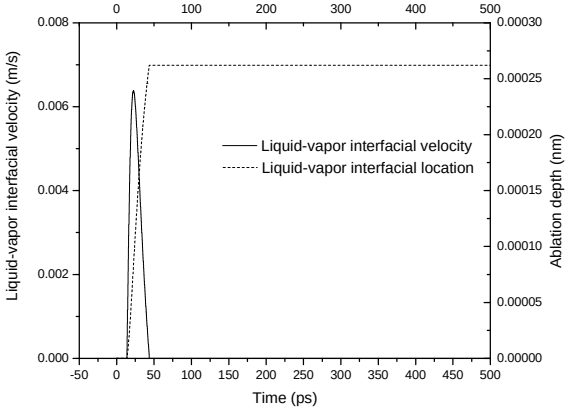

(c) Liquid-vapor interfacial velocity and location

Fig. 3 Irradiation by a 0.5 J/cm^2 single laser pulse

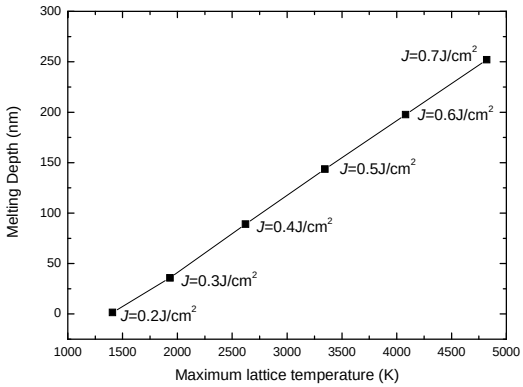

Fig. 4 Dependence of melting depth on maximum lattice temperature

Single pulse irradiations on film with thickness ranged from 500nm to 1100nm were simulated. Three different pulse fluence values were adopted: 0.4 J/cm^2, 0.5 J/cm^2, and 0.6 J/cm^2. The relationship between maximum melting depth and film thickness is shown in Fig. 5. When the thickness decreases lower than 600 nm, the melting depth increases dramatically. However, the film thickness shows very little influence on melting depth when it is greater than 800 nm. This means that within the current range of laser energy, thicker film will act almost the same as bulk gold. The evaporation effects are evaluated by ablation depth. As shown in Fig. 6, the ablation depth is much smaller than melting depth, but its dependence on film thickness is still conclusive. Smaller film thickness will lead to higher ablation depth, which is caused by higher temperature achieved. When the thickness is greater than 1000 nm, its influence on ablation depth is almost negligible.

2. Multiple pulses irradiation

By dividing one single pulse into several consecutive smaller laser pulses, more control can be provided for the laser operation, along with some other advantages as shown below.

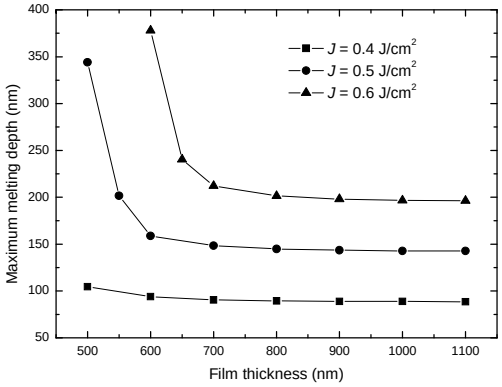

Fig. 5 Dependence of maximum melting depth on film thickness

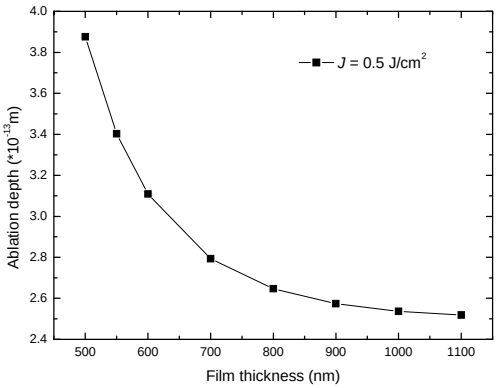

Fig. 6 Dependence of ablation depth on film thickness

First of all, two consecutive pulses with same fluence and a separation time of Δt were studied. The irradiation processes caused by two 0.3 J/cm^2, 100fs laser pulses with a separation time ranged from 10ps to 6000ps are then simulated. The dependence of maximum melting depth on maximum lattice temperature with different separation time is shown in Fig. 7(a). The arrows indicate the directions toward which the separation time Δt increases. The solid line in Fig. 7(a) is the result of single pulse, as shown in Fig. 4. All the results of two pulses are located in the upper side of the solid line, which means that with the same peak temperature, the melting depth of two pulses will always be deeper than that of a single pulse. Furthermore, it can be seen that when the separation time increases from 10 ps, the maximum temperature will decrease without an obvious drop of melting depth. The result points of two pulses deviate from the single pulse line gradually. When the aim of laser irradiation is to obtain deeper melting depth, this is a good trend because the same melting depth can be achieved with lower temperature, i.e., the residual thermal stress will be lower. However, when the separation time is longer than 280ps, the result points of two pulses approach to the single pulse line again, melting depth drops soon with the same temperature. When the separation time equals to 800ps, the difference between two pulses and single pulse is very small. After that, with the increase of separation time, the results caused by two pulses will deviate from the solid line again. After comparing this result with the variation of solid-liquid interface velocity, it was found that 280ps is just the time when the solid-liquid interfacial velocity turn from positive to negative, i.e., when the resolidification process starts; 800ps is the time when the interfacial velocity achieves maximum negative value. This proves that if a deeper melting depth is the aim of laser metal interaction, the second pulse should be launched when the melting process caused by the first pulse reaches the maximum value. On the other hand, if the second pulse is launched when the resolidification process is about to stop, two pulses irradiation shows no advantage over the single pulse.

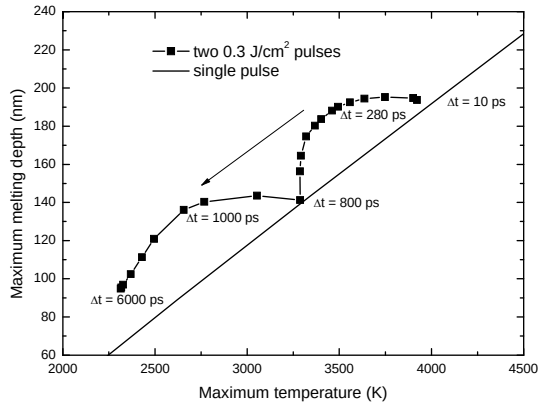

Fig. 7 Relationship between maximum temperature and melting depth

The situations of more than two pulses in one burst are also studied. To be compared with a single pulse of 0.6 J/cm^2, six cases are considered: (a) 2 pulses at 0.3J/cm^2 per pulse; (b) 3 pulses at 0.2J/cm^2 per pulse; (c) 4 pulses at 0.15J/cm^2 per pulse; (d) 5 pulses at 0.12J/cm^2 per pulse; (e) 6 pulses at 0.1J/cm^2 per pulse; (f) 10 pulses at 0.06J/cm^2 per pulse. The separation time ranged from 1ps to 15ps.

Figure 8 and 9 show the dependence of maximum temperature and melting depth on the number of pulses and separation time. It can be seen that with more pulses per burst, the temperature and melting depth will decrease. The increase of separation time also leads to lower temperature and melting depth.

If the relationship between maximum temperature and melting depth caused by multiple pulses is plotted and compared with that of a single pulse, Fig. 10 can be obtained. It is clear that all the points are located on the upper side of the single pulse line, which means deeper melting depth will be achieved with the same lattice temperature. And this difference will be larger with higher number of pulses and longer separation time. In comparison to a single 0.6J/cm^2 pulse irradiation, the maximum lattice temperature caused by 10 consecutive pulses with a separation time of 15ps can reduce 22.01%, while the melting depth only decreases 4.93%. This means in practical application, if deeper melting is wanted, multiple pulses is preferable than single pulse, because it will lead to lower temperature, then smaller residual stress and distortion.

3. Pulse train irradiation

As shown in Fig. 2, a laser pulse train consists of several pulse bursts with a repetition rate of 0.5~1 MHz. Each pulse burst contains 3~10 pulses with an interval of 50 ps ~ 10 ns. To compare the result of pulse train with single pulse, five different single pulse fluences are used: 0.022, 0.026, 0.030, 0.034, and 0.036 J/cm^2. The other parameters are kept the same: repetition frequency 1000 Hz, separation time 100 ps, and 10 pulse bursts.

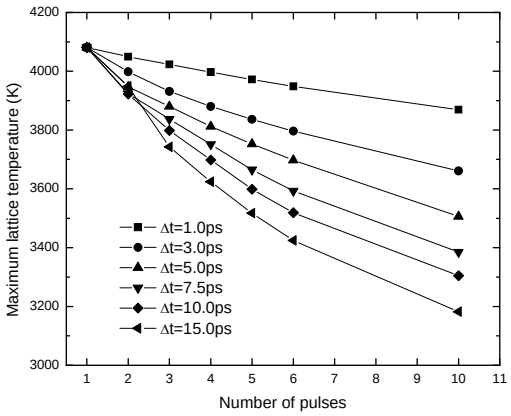

Fig. 8 Dependence of maximum temperature on pulses number and separation time

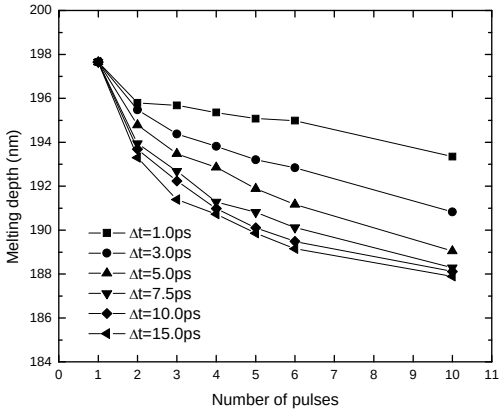

Fig. 9 Dependence of melting depth on pulses number and separation time

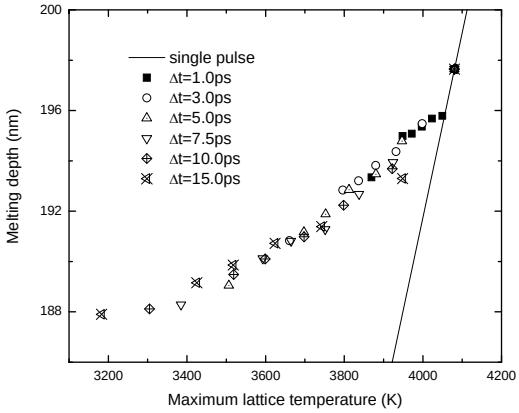

Fig. 10 Comparison of melting depth between multiple pulses irradiation and single pulse irradiation

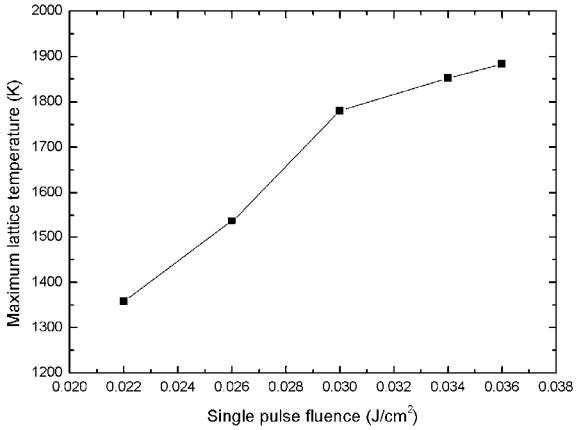

(a) Lattice temperature

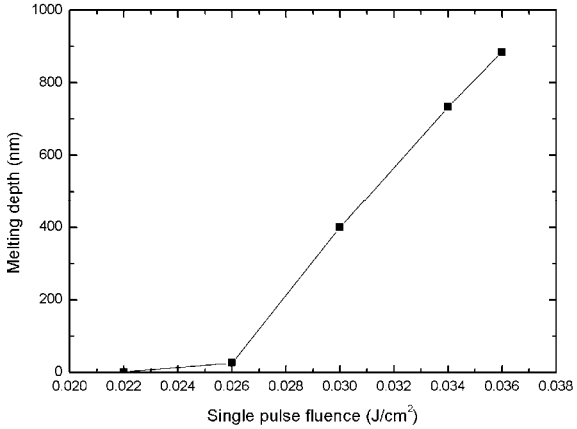

(b) Melting depth

Fig. 11 The effects of single pulse fluence on the irradiation process

The dependence of maximum lattice temperature and melting depth on the fluence is shown in Fig. 11. It is obvious that with higher laser fluence, deeper melting will be achieved and higher temperature will be caused. In the ultrafast laser materials processing, it is desirable that the melting depth can be accurately controlled and the temperature rise should be as low as possible to reduce the thermal stress.

To compare the results of pulse train and single pulse irradiation, the relationship between the maximum lattice temperature and melting depth is shown in Fig. 12. The lower line is single pulse while the upper one is for pulse train. With the increase of pulse train power, the melting depth increases rapidly while the maximum lattice temperature increased relatively slowly. It is clear that with the same lattice temperature, the melting depth caused by pulse trains is much deeper than that caused by the single pulse. For example, the highest lattice temperature caused by a single 0.3 J/cm^2 pulse irradiation is almost the same as pulse trains which consists of 10 trains with 3 single 0.036 J/cm^2-pulses in a train, but its melting depth is only 50 nm, much less than the melting caused by the pulse train, almost 900 nm. On the other hand, to achieve the same melting depth, a pulse train will cause much lower lattice temperature, which is an advantage for laser-materials processing. However, the energy needed for a pulse train is much higher that of a single pulse. According to Fig. 12, the melting depth caused by a single 0.3 J/cm^2 pulse is almost the same as the pulse train which consists of 10 bursts with 3 single 0.026 J/cm^2 pulses in a burst. But the total energy for the pulse train is 0.78J/cm^2. This is because more energy is used to heat up the deeper part of the film for the case of pulse train.

It should be noted that in Fig. 12 the lattice temperatures for laser train mode irradiation never reach 2000K, far blow the normal boiling point of gold, 3127 K. This is true for all the calculations in this paper. Before the lattice temperature reaches 3127 K, the whole film will be melted, at which point the calculation will stop.

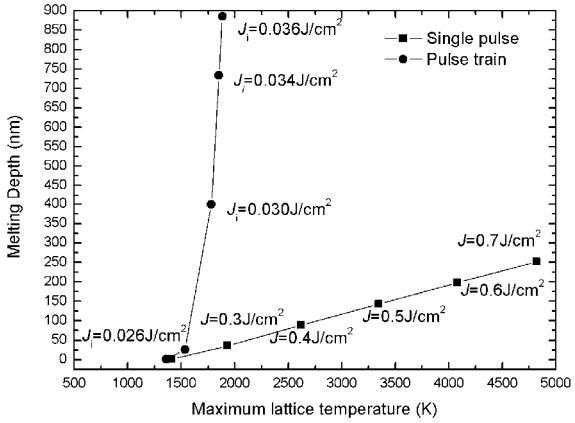

Fig. 12 The relationship between melting depth and maximum temperature, comparison between single pulse and pulse train

Another issue to be addressed is the heat loss at surface. In most computational study on laser metal interaction, the heat loss at boundaries was neglected, which is proved to be reasonable in our earlier work [25]. But for pulse train irradiation, the time scale is much larger in orders. The pulse train with a repetition rate of 1000 Hz has a time scale 10^{10} times larger than a typical 100-femtosecond laser pulse. Under this condition, the radiation caused heat loss may play a more important role in the process. Two computations were carried out: one with adiabatic boundary condition while another includes the radiation heat loss at the boundary. The comparison between maximum lattice temperatures shows no obvious difference. But because the radiation at the surface will cause laser energy to escape from the film, the melting depth will be smaller than the results estimated by models ignoring this factor, as shown in Fig. 13. This means neglecting heat loss at surface will lead to an overestimation on melting depth when the repetition rate is low enough.

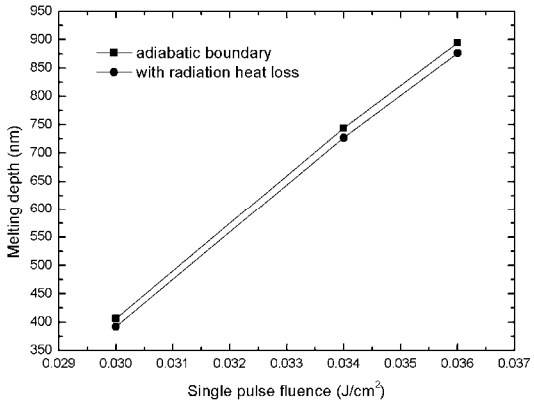

Fig. 13 The effects of heat loss on melting depth

From the above discussion, the merits of pulse train can be seen clearly. But to utilize laser pulse trains, there are more parameters to be controlled than a single pulse irradiation did, such as the repetition rate. Typical repetition rate for femtosecond lasers ranges from 100 Hz to tens of MHz. Numerical simulations are carried out for eight frequencies between 500 Hz and 1 MHz and different pulse fluence, and the results are shown in Fig. 14. It is clear that repetition rate has little effects on the maximum melting depth. This is because even for a high repetition rate as 1 MHz, there is still enough time between each train for the heat to transfer in the thin film and the melting depth will mainly be decided by the amount of energy deposited on the film.

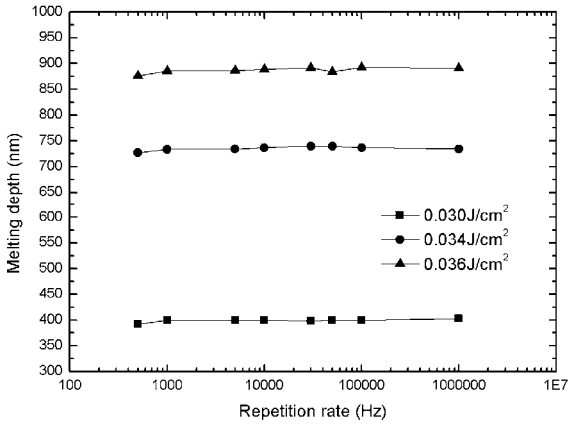

(b) Melting depth

Fig. 14 The effects of repetition rate

CONCLUSION

The entire process of laser-metal interaction – including preheating, melting, vaporization, resolidification and thermalization – was thoroughly investigated under the frame works of two-temperature model and interfacial tracking method. Three modes of laser pulses – including single pulse, multiple pulses and pulse train – were used in the simulation to study the effects of various parameters on the maximum lattice temperature, melting depth and ablation depth.

(1) Simulations on single pulse irradiation show that The results show that higher laser fluence *J* leads to higher liquid-vapor interface temperature, velocity and deeper ablation depth. The ablation depth is very small in comparison with the film thickness and melting depth. The effects of laser fluence on solid-liquid interface are also studied and the results show the same tendency as for liquid-vapor interface. However, the solid-liquid interfacial velocity is much higher.

(2) The calculations on films with different thickness show that when the thickness is less than 600 nm, melting depth increases significantly. With the laser fluence of 0.5 J/cm^2, the melting depth doubles when film thickness increases from 600 nm to 500 nm. However, when film thickness is larger than 800 nm, film thickness shows little influence on melting depth.

(3) For two pulses irradiation, if deeper melting depth is wanted, the second pulse should be launched when the melting depth caused by first pulse reaches the peak. In comparison to single pulse irradiation with the same lattice temperature, this will lead to a greater melting depth. If the second pulse is launched at the time when the resolidification process is about to end, two pulses irradiation shows no difference to a single pulse process. For ablation caused by evaporation, if the second pulse is launched during the surface temperature reaches the peak, ablation depth will be smaller than a single pulse.

(4) For laser irradiation with more than two consecutive pulses, if the total laser fluence remains a constant, higher pulse number and longer separation times between pulses will lead to smaller melting depth, but in comparison with a single pulse that causes the same lattice temperature, the melting depth is much deeper. At the same time, multiple pulses irradiation shows no advantage in ablation over single pulse with the same peak temperature.

(5) Compared to single-pulse irradiation, laser pulse train showed good performance in achieving deeper melting depth, especially in higher laser power. The temperature rise caused by laser irradiation increases relatively slowly with the increase of total laser energy deposited on the film. Repetition rate has little influence on the process. With the repetition rate ranges of 500 Hz to 1 MHz, the maximum lattice temperature and melting depth showed little change with all other parameters kept unchanged;

ACKNOWLEDGMENTS

Support for this work by the U.S. National Science Foundation (NSF) under Grant No. CBET-0730143 and Chinese National Natural Science Foundation under Grant No. 50828601 is gratefully acknowledged.

REFERENCES

[1]. Wang, G. X. and Prasad, V., 2000, "Microscale heat and mass transfer and non-equilibrium phase change in rapid solidification," Materials Science and Engineering A, 292(2): pp. 142-148.

[2]. Hohlfeld, J., Wellershoff, S. S., Gudde, J., Conrad, U., Jahnke, V., and Matthias, E., 2000, "Electron and lattice dynamics following optical excitation of metals," Chemical Physics, 251(1-3): pp. 237-258.

[3]. Groeneveld, R. H. M., Sprik, R., and Lagendijk, A., 1995, "Femtosecond spectroscopy of electron-electron and electron-phonon energy relaxation in ag and au," Physical Review B, 51(17): pp. 11433-11445.

[4]. Furukawa, H. and Hashida, M., 2002, "Simulation on femto-second laser ablation," Applied Surface Science, 197-198: pp. 114-117.

[5]. Furusawa, K., Takahashi, K., Kumagai, H., Midorikawa, K., and Obara, M., 1999, "Ablation characteristics of au, ag, and cu metals using a femtosecond ti:Sapphire laser," Applied Physics A: Materials Science and Processing, 69(7): pp. S359-S366.

[6]. Corkum, P. B., Brunel, F., Sherman, N. K., and Srinivasan-Rao, T., 1988, "Thermal response of metals to ultrashort-pulse laser excitation," Physical Review Letters, 61(25): pp. 2886-2889.

[7]. Anisimov, S. I., Kapeliovich, B. L., and Perel'man, T. L., 1974, "Electron emission from metal surfaces exposed to ultra-short laser pulses," Soviet Physics - JETP, 39(2): pp. 375-377.

[8]. Qiu, T. Q. and Tien, C. L., 1993, "Heat transfer mechanisms during short-pulse laser heating of metals," Journal of Heat Transfer, ASME, 115(4): pp. 835-841.

[9]. Tzou, D. Y., *Macro- to microscalse heat transfer*, 1997, Taylor & Francis: Washington, D.C.

[10]. Tzou, D. Y., *Computational techniques for microscale heat transfer*, in Handbook of numerical heat transfer, 2nd ed., W.J. Minkowycz, E.M. Sparrow, and J.Y. Murthy, Editors. 2006, Wiley, Hoboken, NJ.

[11]. Jiang, L. and Tsai, H. L., 2005, "Improved two-temperature model and its application in ultrashort laser heating of metal films," Journal of Heat Transfer, 127(10): pp. 1167-1173.

[12]. Chen, J. K., Tzou, D. Y., and Beraun, J. E., 2006, "A semiclassical two-temperature model for ultrafast laser heating," International Journal of Heat and Mass Transfer, 49(1-2): pp. 307-316.

[13]. Von Der Linde, D., Fabricius, N., Danielzik, B., and Bonkhofer, T., 1987, "Solid phase superheating during picosecond laser melting of gallium arsenide," *Materials Research Society Symposia Proceedings*.

[14]. Zhang, Y. and Chen, J. K., 2008, "An interfacial tracking method for ultrashort pulse laser melting and resolidification of a thin metal film," Journal of Heat Transfer, 130(6): pp. 0624011-06240110.

[15]. Chen, J. K., Latham, W. P., and Beraun, J. E., 2005, "The role of electron-phonon coupling in ultrafast laser heating," Journal of Laser Applications, 17(1): pp. 63-68.

[16]. Chowdhury, I. H. and Xu, X., 2003, "Heat transfer in femtosecond laser processing of metal," Numerical Heat Transfer; Part A: Applications, 44(3): pp. 219-232.

[17]. Anisimov, S. I. and Rethfeld, B., 1997, "Theory of ultrashort laser pulse interaction with a metal," *Proceedings of SPIE Vol 3093*.

[18]. Kuo, L.-S. and Qiu, T., 1996, "Microscale energy transfer during picosecond laser melting of metal films," *ASME Natl. Heat Transfer Conf.*

[19]. Klemens, P. G. and Williams, R. K., 1986, "Thermal conductivity of metals and alloys," Int. metals reviews, 31(5): pp. 197-215.

[20]. Faghri, A. and Zhang, Y., *Transport phenomena in multiphase systems*, 2006, Elsevier Academic Press: Burlington, MA.

[21]. Xu, X., Chen, G., and Song, K. H., 1999, "Experimental and numerical investigation of heat transfer and phase change phenomena during excimer laser interaction with nickel," Int. J. Heat Mass Transfer, 42(8): pp. 1371-1382.

[22]. Birks, N., Meier, G. H., and Pettit, F. S., *Introduction to the high-temperature oxidation of metals, second ed.*, 2006, Cambridge University Press: Cambridge.

[23]. Akhatov, I., Lindau, O., Topolnikov, A., Mettin, R., Vakhitova, N., and Lauterborn, W., 2001, "Collapse and rebound of a laser-induced cavitation bubble," Phys. Fluids, 13(10): pp. 2805-2819.

[24]. Huang, J., Zhang, Y., and Chen, J. K., 2009, "Ultrafast solid-liquid-vapor phase change in a thin gold film irradiated by multiple femtosecond laser pulses," Int. J. Heat Mass Transfer, 52(13-14): pp. 3091-3100.

[25]. Huang, J., Zhang, Y., and Chen, J. K., 2009, "Ultrafast solid-liquid-vapor phase change of a gold film induced by pico- to femtosecond lasers," Appl. Phys. A - Mater., 95(3): pp. 643-653.

[26]. Patankar, S., *Numerical heat transfer and fluid flow*, 1980, Taylor & Francis.

[27]. Barin, I., *Thermochemical data of pure substance, part i*, 1993, VCH: New York.